# Aeroelastic Instabilities of FGM Panels under Thermo-Mechanical Loads

# AEROELASTIC INSTABILITIES OF FGM PANELS UNDER THERMO-MECHANICAL LOADS

**E. Carrera[1], E. Zappino[2], and M. Cinefra[3]**

[1] *Politecnico di Torino, DIMEAS, C.so Duca degli Abruzzi, 24; e-mail:erasmo.carrera@polito.it.*

[2] *Politecnico di Torino, DIMEAS, C.so Duca degli Abruzzi, 24; e-mail:enrico.zappino@polito.it.*

[3] *Politecnico di Torino, DIMEAS, C.so Duca degli Abruzzi, 24; e-mail:maria.cinefra@polito.it.*

## ABSTRACT

The aero-thermo-elastic analysis of functionally graded material is presented in this paper. A unified approach based on the Carrera unified formulatin has been used to derive the model using a compact notation. Refined two-dimensional theories have been used as structural model while the piston theory has been used to evaluate the aerodynamic forces, therefore only supersonic velocities have been considered. The in-plane normal stresse due to the thermal load have been included in the analysis. The present model has been used to analyze FGM panel considering different boundary conditions and material configurations. The model is able to investigate both panel flutter and thermal buckling instabilities. The results, compared with those from literature, confirm the ccuracy of the model. The instability boundaries of different FGM panel have been investigated and compared.

Key words: Panel Flutter, FGM, Aero-thermo-elasticity.

## 1. INTRODUCTION

Panel flutter is an aeroelastic phenomenon that can cause failure of panels of wings, fuselages and missiles. It happens mostly at supersonic regime even though it can be observed in subsonic ranges. The panel flutter phenomena may appear in space structures during the coasting phase. Some non-destructive aeroelastic phenomena were detected on Saturn V rockets, and analytical and experimental test was carried out as shown by Nichols [1]. The new launchers generation requires the use of thermal protections able to preserve the structural integrity during the coasting phase when the structures are subject to thermal, mechanical and aerodynamic loads. Some numerical and experimental investigations on the aeroelastic response of thermal insulation panels were performed during the Future Launchers Preparatory Program, FLPP, promoted by the Europe Space Agency, ESA. The results, [2, 3], show that the design of such structure has to include the aeroelastic behaviour because panel flutter may occur during the atmospheric flight of spacecraft. The work by Carrera and Zappino[4] present a numerical approach to the solution of this problem using a refined beam model. The introduction of advanced materials, such as the Functionally Graded Material (FGM), allows the requirements of mechanical strength and thermal protection to be fulfilled. The thermo-mechanical properties of the FGM are variable through the thickness without discontinuity such as in the composite or sandwich materials. The analysis of FGM panels requires the use of advanced structural models [5, 6, 7] because they take into account the deformation through the thickness of the panel while classical model neglect it. In this work, the aero-thermo-mechanical analysis of FGM panels is performed by using a refined shell theory [7, 8]. Both the structural model, including the thermal effects, and the aerodynamic model, based on the piston theory [9] in its linear formulation, are derived in the framework of the Carrera Unified Formulation CUF [10]. Equivalent Single Layer (ESL) and Layer Wise (LW) models are considered. The effects of the thermal load and the influence of the FGM properties on the aeroelastic instability are investigated. Only supersonic regimes are considered in according with the Piston theory assumptions. The results show that the thermal loads can deeply afflict the aeroelastic behaviour of the panel. The use of the refined shell elements appears to be mandatory for the analysis of such structures.

## 2. AERO-THERMO-ELASTIC MODEL

The aero-thermo-elastic model used in the present paper can be written in its general formulation usingthe Principle of Virtual Displacements, PVD:

$$\delta L_{int} + \delta L_{ine} + \delta L_{\sigma^T} = \delta L_{ext} \qquad (1)$$

where: $L_{int}$ is the internal virtual work due to the elastic forces, $L_{ine}$ is the work due to the inertial forces, and $L_{ext}$ is the work due to the external forces; $\delta$ denotes virtual variations. If none of the external loads, except the aerodynamic forces, are considered, the terms $\delta L_{ext}$ can be written as $\delta L_a$ where $L_a$ stands for the work of the aerodynamic loads.
$L_{\sigma^T}$ is the work done by the initial stress distribution due to the thermal load. If the FEM is used to solve the problem, the virtual works can be written in matrix form. Equation 1 therefore becomes:

$$\left([\boldsymbol{K}] + [\boldsymbol{K}_a] + [\boldsymbol{K}_{\boldsymbol{\sigma}^T}]\right)\{\boldsymbol{q}\} + [\boldsymbol{D}_a]\{\dot{\boldsymbol{q}}\} + [\boldsymbol{M}]\{\ddot{\boldsymbol{q}}\} = 0 \quad (2)$$

where $[K]$ is the stiffness matrix, $[M]$ is the mass matrix, $[Ka]$ is the aerodynamic stiffness matrix and $[Da]$ is the aerodynamic damping matrix. $[K_{\sigma^T}]$ is the geometrical stiffness due ti the thermal load. The structural damping and the flow inertia can be neglected. Each of these matrices is derived in explicit form in the following sections. The solution of Eq.2 in the frequency domain leads to the solution of a Quadratic Eigenvalues Problem (QEP). The details of the solution approach are herein omitted for the sake of brevity, but can be found in the work by Carrera and Zappino [4].

## 2.1. Advanced plate elements

The refined plate model used in the present paper is derived using the Carrera Unified Formulation (CUF). when a two-dimensional formulation is considered, a generic three-dimensional displacement field can be expressed as a contribution on the reference surface and a contribution on the thickness. The displacement field assumes the following formula:

$$\boldsymbol{u}^k(x,y,z) = F_\tau(z)\boldsymbol{u}^k_\tau(y,x) \qquad \tau, s = 1, ..., N \quad (3)$$

where $(x, y, z)$ is the cartesian reference system and $k$ identifies the layer. $F_\tau$ is the so-called thickness function which only depends on $z$, and it is used to approximate the thickness deformation. The choice of $F_\tau$ is discussed above, $\tau$ goes from 1 to $N$ where $N$ is the number of terms in the expansion. The function $\boldsymbol{u}^k_\tau(x, y)$ can be approximated with the FEM method. If the shape functions are denoted with $N_i$, the Equation 3 becomes:

$$\boldsymbol{u}^k(x,y,z) = F_\tau(z)N_i(x,y)\boldsymbol{q}^k_{i\tau} \quad (4)$$
$$\tau = 1, ..., N; \quad i = 1, ..., N_n$$

where $N_n$ is the number of nodes used in the finite element formulation. The virtual variation of displacement can be expressed as:

$$\delta\boldsymbol{u}^k(x,y,z) = F_s(z)N_j(x,y)\delta\boldsymbol{q}^k_{js} \quad (5)$$
$$s = 1, ..., N;\ j = 1, ..., N_n \quad (6)$$

The thickness functions ($F_\tau$ and $F_s$) and the Finite element formulation ($N_i$ and $N_j$) are discussed in the following sections.

### 2.1.1. Thickness approximation (CUF)

Many different functions can be chosen to approximate the thickness deformation. Two different approaches are here dealt with: the Equivalent Single Layer (ESL) and the Layer-Wise (LW) approximation.
In the case of Equivalent Single Layer (ESL) models, a Taylor expansion is employed as the thickness functions:

$$F_\tau\boldsymbol{u}_\tau = \sum_{\tau=1}^{N} z^{\tau-1}\boldsymbol{u}_{\tau-1} = z^0\boldsymbol{u}_0 + z^1\boldsymbol{u}_1 + \ldots + \\ + \ldots + z^{N-1}\boldsymbol{u}_{N-1} \quad (7)$$

In the case of Layer-Wise (LW) models, the displacement is defined at a $k$-layer level:

$$F_\tau\boldsymbol{u}^k_\tau = F_t\,\boldsymbol{u}^k_t + F_b\,\boldsymbol{u}^k_b + F_r\,\boldsymbol{u}^k_r\,\boldsymbol{u}^k_s, \\ \tau = t, b, r\ , \quad r = 2, ..., N. \quad (8)$$

$$F_t = \frac{P_0 + P_1}{2}, \quad F_b = \frac{P_0 - P_1}{2}, \quad F_r = P_r - P_{r-2}. \quad (9)$$

in which $P_j = P_j(\zeta_k)$ is the Legendre polynomial of the $j$-order defined in the $\zeta_k$-domain: $-1 \leqslant \zeta_k \leqslant 1$. The top ($t$) and bottom ($b$) values of the displacements are used as unknown variables and the following compatibility conditions can be imposed:

$$u^k_t = u^{k+1}_b, \qquad k = 1, N_l - 1. \quad (10)$$

The LW models, with respect to the ESLs, allow the zig-zag form of the displacement distribution in layered structures to be modelled. In this paper the models based on the ESL approach will be indicated using the acronym $ESL - N$ where $N$ is the number of terms of the expansion. The LW models will be named using $LW - N$ where $N$ is the number of terms of the expansion in each layer. As example, an ESL2 model is a linear ELS model while and LW3 is a quadratic LW model.

### 2.1.2. FEM approximation

The FEM is used to approximate the solution over the reference surface. It allows the unknowns $u^k_\tau$, introduced in equation 4, to be written as follows:

$$\boldsymbol{u}^k_\tau(x,y) = N_i(x,y)\boldsymbol{q}^k_{i\tau}\ \tau = 1, ..., N; \quad i = 1, ..., N_n,$$

where $N_i$ are the FEM shape functions. The index $i$ denotes the node in which the function is centred.

In the case of a 9-node element, the shape functions are written as:

$$\begin{aligned}
N_1 =& \frac{1}{4}\Big(\xi^2-\xi\Big)\Big(\eta^2-\eta\Big)\\
N_2 =& \frac{1}{2}\Big(1-\xi^2\Big)\Big(\eta^2-\eta\Big)\\
N_3 =& \frac{1}{4}\Big(\xi^2+\xi\Big)\Big(\eta^2-\eta\Big)\\
N_4 =& \frac{1}{2}\Big(\xi^2+\xi\Big)\Big(1-\eta^2\Big)\\
N_5 =& \frac{1}{4}\Big(\xi^2+\xi\Big)\Big(\eta^2+\eta\Big)\\
N_6 =& \frac{1}{2}\Big(1-\xi^2\Big)\Big(\eta^2+\eta\Big)\\
N_7 =& \frac{1}{4}\Big(\xi^2-\xi\Big)\Big(\eta^2+\eta\Big)\\
N_8 =& \frac{1}{2}\Big(\xi^2-\xi\Big)\Big(1-\eta^2\Big)\\
N_9 =& \Big(1-\xi^2\Big)\Big(1-\eta^2\Big)
\end{aligned} \tag{11}$$

The membrane and shear locking are here corrected using the Mixed Interpolation of Tensorial Components technique, MITC9. This approach allows the strain components to be computed using an interpolation of the strain over the element instead deriving them directly from the displacements. The details of the MITC9 approach are not reported for sake of brevity, but can be found in the work by Cinefra *et al.* [8]

#### 2.1.3. Stress and strain formulation

The strain vector can be written as:

$$\boldsymbol{\varepsilon} = (\varepsilon_{xx}\ \varepsilon_{yy}\ \varepsilon_{xy}\ \varepsilon_{xz}\ \varepsilon_{yz}\ \varepsilon_{zz})^T \tag{12}$$

It can be written in terms of displacements using the relation:

$$\boldsymbol{\varepsilon} = \boldsymbol{D}\boldsymbol{u} \tag{13}$$

The matrix $[D]$ contains the geometrical relations between the displacements and the strains. In this case, matrix $\boldsymbol{D}$ is also a function of the interpolation functions introduced by the MITC9 technique. The explicit form of matrix $\boldsymbol{D}$ can be found in the works by Cinefra *et al.* [8], or in the book by Carrera *et al.* [10]. The stress vector can be derived using the constitutive equations,

$$\boldsymbol{\sigma} = \boldsymbol{C}^k(z)\boldsymbol{\varepsilon} \tag{14}$$

where $\boldsymbol{C}^k(z)$ is the matrix of the material coefficients and $\boldsymbol{\sigma}$ is the stress vector,

$$\boldsymbol{\sigma} = (\sigma_{xx}\ \sigma_{yy}\ \sigma_{xy}\ \sigma_{xz}\ \sigma_{yz}\ \sigma_{zz})^T \tag{15}$$

when FGM materials are considered the material coefficients must be considered variable through the thickness in according with the FGM variation law. in the next section the FGM properties will be discussed deeply.

#### 2.1.4. Thermal stresses

The initial thermal stresses can be written as:

$$\sigma^{\theta}_{xx} = \lambda_{xx}\Delta T; \sigma^{\theta}_{yy} = \lambda_{yy}\Delta T, \tag{16}$$

Where $\Delta T$ is the temperature change. The coefficients $\lambda$ can be obtained from the formulation:

$$\begin{bmatrix} \sigma^{\theta}_{xx} \\ \sigma^{\theta}_{yy} \end{bmatrix} = \begin{bmatrix} C_{11} & C_{12} & C_{16} \\ C_{21} & C_{22} & C_{26} \end{bmatrix} \begin{bmatrix} \alpha_{xx}(z) \\ \alpha_{yy}(z) \\ \alpha_{xy}(z) \end{bmatrix} \tag{17}$$

where $\alpha$ denotes the thermal expansion coefficients that, when FGM materials are considered, must be considered not constant through the thickness.

#### 2.1.5. Elastic Work: Stiffness Matrix $[K]$

The internal work, $\delta L_{int}$, can be expressed in terms of elastic energy using the equations introduced in the section above.

$$\begin{aligned}
\delta L_{int} =& \int_V (\delta\boldsymbol{\varepsilon}^T\boldsymbol{\sigma})dV = \\
&= \delta\mathbf{q}^{k^T}_{\tau i}\Big[\int_V \boldsymbol{D}^T\Big(N_i(x,y)F_\tau(z)\boldsymbol{I}\Big)\boldsymbol{C}^k(z)\\
&\Big(N_j(x,y)F_s(z)\boldsymbol{I}\Big)\boldsymbol{D}dV\Big]\mathbf{q}^k_{sj}
\end{aligned} \tag{18}$$

The variation of the internal work can be written, in terms of the fundamental nucleus of the stiffness matrix, as follows:

$$\delta L_{int} = \delta\mathbf{q}^{k^T}_{\tau i}\mathbf{k}^{ij\tau s}\mathbf{q}^k_{sj} \tag{19}$$

where $\mathbf{k}^{ij\tau s}$ is the stiffness matrix in the form of the fundamental nucleus. The explicit forms of the 9 components of $\mathbf{k}^{ij\tau s}$can be found in the book by Carrera *et al.* [10].

#### 2.1.6. Inertial Work: Mass Matrix $[M]$

The mass matrix formulation id derived from the variation of the work made by the inertial forces:

$$\delta L_{ine} = \int_V \delta\mathbf{u}^k\cdot\ddot{\mathbf{u}}^k\cdot\rho^k(z)dV \tag{20}$$

where the dot denotes derivatives with respect to time and the double dot denotes acceleration. After substitution of eq.5 in eq.20, one obtains:

$$\begin{aligned}
\delta L_{ine} =& \delta\mathbf{q}^{k^T}_{i\tau}\Big[\int_V\Big(F_\tau(z)\boldsymbol{I}N_i(x,y)\rho^k(z)\\
&N_j(x,y)F_s(z)\boldsymbol{I}\Big)dV\Big]\ddot{\mathbf{q}}^k_{sj} =\\
=& \delta\mathbf{q}^{k^T}_{i\tau}\mathbf{m}^{ij\tau s}\ddot{\mathbf{q}}^k_{sj}
\end{aligned} \tag{21}$$

where $\mathbf{m}^{kij\tau s}$ is the mass matrix, which is a function of the shape functions $N_i$, $F_\tau$ and of the material density $\rho^k(z)$, which is not constant through the layers thickness.

#### 2.1.7. Initial thermal stress $[K^\theta_\sigma]$

The effects of the initial thermal stress can be included in the analysis considering the work done by the variation of the virtual non-linear strain, $\varepsilon_{nl}$, given by the von Karman Formulation, with the thermal initial stress, $\sigma^\theta$.:

$$\delta L_{\sigma^\theta} = \int_V (\delta\varepsilon_{xx_{nl}}\sigma^\theta_{xx}) + (\delta\varepsilon_{yy_{nl}}\sigma^\theta_{yy})dV \tag{22}$$

when only the in-plane stresses are considered, the fundamental nucleus becomes:

$$\begin{aligned}\delta L_{\sigma^\theta} &= \delta\mathbf{q}_{i\tau}\Big[\Delta T \\ &\int_V \Big(F_\tau(z)\boldsymbol{I}N_{i,x}(x,y)\lambda^k_{xx}(z)N_{j,x}(x,y)\boldsymbol{I}F_s(z)+ \\ &\Big(F_\tau(z)\boldsymbol{I}N_{i,y}(x,y)\lambda^k_{yy}(z)N_{j,y}(x,y)\boldsymbol{I}F_s(z)\Big)dV\Big]\mathbf{q}_{sj} = \\ &= \delta\mathbf{q}_{i\tau}\Delta T{\boldsymbol{k}_{\boldsymbol{\sigma^\theta}}}^{kij\tau s}\mathbf{q}_{sj}\end{aligned} \tag{23}$$

Where ${\boldsymbol{k}_{\boldsymbol{\sigma^\theta}}}^{kij\tau s}$ is the fundamental nucleus of the stiffness matrix due to the initial thermal stress.

### 2.2. Aerodynamic model

The aerodynamic model used in the present work is based on the Piston Theory. This model was first used in aeroelastic analysis by Ashley and Zartarian [9]; it has an easy formulation and it provides accurate results in the supersonic range, for Mach numbers greater than 1.7. The piston theory assumes that the flow on a panel is similar at a one-dimensional flow in a channel (e.g. in a piston). The flow velocity is assumed to be parallel to the surface and the vertical velocity $\dot{u}_z$ can therefore be expressed in two dimensional from as:

$$\dot{u}_z = \frac{\partial u_z}{\partial t} \pm V_\infty \frac{\partial u_z}{\partial x} \tag{24}$$

There are two contributions: the former is due to the vertical displacement, and the latter is due to the surface slope. The sign of velocity $V_\infty$ depends on its direction: it is positive if $V_\infty$ is in the positive $x-direction$ and negative if $V_\infty$ is in the negative $x-direction$. The differential pressure across a panel can therefore be expressed as:

$$\Delta p(\alpha,t) = \frac{2q}{M}\Big\{\frac{\partial u_z}{\partial x} + \frac{1}{V_\infty}\frac{\partial u_z}{\partial t}\Big\}. \tag{25}$$

Eq.25 shows that the local differential pressure is a function of the velocity of the normal displacement and of the slope of the surface. A refined formulation has been proposed by Krumhaar [11] for low supersonic ranges:

$$\Delta p(y,t) = \frac{2q}{\sqrt{M^2-1}}\Big\{\frac{\partial u_z}{\partial x} + \frac{M^2-2}{M^2-1}\frac{1}{V_\infty}\frac{\partial u_z}{\partial t}\Big\} \tag{26}$$

It is easy to see that when the Mach number goes to infinity, the eq.26 coincides with eq.25. In this work, eq.26 is used to compute the virtual work related to the aerodynamic forces. The differential pressure, acting on the panel, given by eq.26, can be expressed as the sum of two terms:

$$\Delta p(y,t) = \pm A\frac{\partial u_z}{\partial x} + B\frac{\partial u_z}{\partial t} \tag{27}$$

where:

$$A = \pm\frac{2q}{\sqrt{M^2-1}}; \qquad B = \frac{2q}{\sqrt{M^2-1}}\frac{M^2-2}{M^2-1}\frac{1}{V_\infty}. \tag{28}$$

The first term, $(\pm A\frac{\partial u_z}{\partial\alpha})$, represents a contribution to the stiffness of the problem, and it is therefore called *aerodynamic stiffness.* The second term, $(B\frac{\partial u_z}{\partial t})$, depends on the vertical velocity and it may be interpreted as a damping; it is therefore called *aerodynamic damping.*

#### 2.2.1. Aerodynamic Stiffness Matrix $[K_a]$

The aerodynamic stiffness matrix may be derived by evaluating the work, $\delta L_{aer}$, made by a differential pressure, $\Delta p$, due to the slope of the surface in the flow direction.

$$\delta L^A_{aer} = \int_\Lambda (\delta\mathbf{u}^k\Delta p^A)\, d\Lambda \tag{29}$$

where index $A$ indicates that only the contribution of the slope is considered, and $\Lambda$ is the surface where the pressure acts. Considering the formulation proposed in eq.27, and introducing the displacement formulation reported in eq.5, differential pressure can be written as:

$$\Delta p^A = A\frac{\partial u_z}{\partial x} = A\cdot I_{\Delta p}\frac{\partial N_i}{\partial x}F_\tau q^k_{i\tau} \tag{30}$$

where:

$$I_{\Delta p} = \begin{bmatrix} 0 & 0 & 0 \\ 0 & 0 & 0 \\ 0 & 0 & 1 \end{bmatrix} \tag{31}$$

Since $d\Lambda = d\alpha\cdot d\beta$, and substituting eq.30 in eq.29, the virtual work of the differential pressure can be written as:

$$\delta L^A_{aer} = \delta q^{k^T}_{js} \left[ A\big(F_s F_\tau\big) \int_\Lambda N_j \frac{\partial N_i}{\partial x} I_{\Delta p}\, d\alpha d\beta \right] q^k_{i\tau} = \delta q^{k^T}_{js}\, \boldsymbol{k}^{kij\tau s}_a q^k_{i\tau} \tag{32}$$

where $\mathbf{k}^{kij\tau s}_a$ is the aerodynamic stiffness matrix which may be written in the form:

$$\boldsymbol{k}^{kij\tau s}_a = \frac{2q}{\sqrt{M^2-1}} F_\tau F_s \begin{bmatrix} 0 & 0 & 0 \\ 0 & 0 & 0 \\ 0 & 0 & \displaystyle\int_\Lambda N_j \frac{\partial N_i}{\partial x}\, dxdy \end{bmatrix} \tag{33}$$

#### 2.2.2. Aerodynamic Damping Matrix $[D_a]$

The aerodynamic damping matrix may be derived by evaluating the work, $\delta L_{aer}$, made by a differential pressure, $\Delta p$, due to the vertical displacement velocity of the surface.

$$\delta L^B_{aer} = \int_\Lambda (\delta \mathbf{u}^k \Delta p^B)\, d\Lambda \tag{34}$$

where index $B$ indicates that only the contribution of the vertical displacement velocity is considered. Considering the formulation proposed in eq.27 and introducing the displacement formulation reported in eq.5 , differential pressure can be written as:

$$\Delta p^B = B \frac{\partial u^k_z}{\partial t} = B \cdot F_\tau N_i I_{\Delta p} \frac{\partial q^k_{i\tau}}{\partial t} \tag{35}$$

$$\delta L^B_{aer} = \delta q^{k^T}_{js} \left[ B\big(F_\tau F_s\big) \int_\Lambda N_i N_j I_{\Delta p}\, d\alpha d\beta \right] \frac{\partial q^k_{i\tau}}{\partial t} = \delta q^{k^T}_{js}\, \boldsymbol{d}^{kij\tau s}_a \frac{\partial q^k_{i\tau}}{\partial t} \tag{36}$$

where $\mathbf{D}^{ij\tau s}_a$ is the aerodynamic damping matrix which may be written in the following form:

$$\boldsymbol{d}^{kij\tau s}_a = \frac{2q}{\sqrt{M^2-1}} \frac{1}{V_\infty} \Big(\frac{M^2-2}{M^2-1}\Big) \int_x \big(F_\tau F_s\big)\, dx \begin{bmatrix} 0 & 0 & 0 \\ 0 & 0 & 0 \\ 0 & 0 & \displaystyle\int_\Lambda N_i N_j\, d\alpha d\beta \end{bmatrix} \tag{37}$$

## 3. NUMERICAL RESULTS

This section shows some results obtained using the aero-thermo-elastic model introduced in the sections above. Different FGM material are considered but all of them are built using two materials, aluminium as metallic and alumina as ceramic, the mechanical and thermal properties are reported in Table 3.

| | Aluminium | Alumina | |
|---|---|---|---|
| $E$ | 70 | 380 | $Gpa$ |
| $\nu$ | 0.3 | 0.3 | - |
| $\rho$ | 2700 | 3940 | $Kg/m^3$ |
| $\alpha$ | $23\times10^{-6}$ | $7.4\times10^{-6}$ | $1/K$ |

The volume fraction formulation used in the present model is

$$V_c = \left(\frac{z}{h} + \frac{1}{2}\right)^{n_g} \tag{38}$$

where $n_g$ is the volume fraction index. Figure 1 show the behaviour of the parameter $V_c$ for different values of $n_g$.

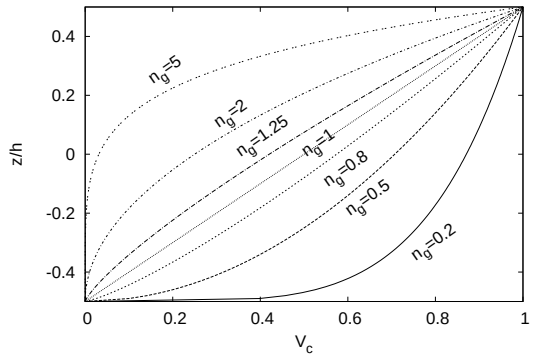


*Figure 1. Volume fraction behaviour for different values of volume fraction index.*

Three different analysis are performed. The thermo-elastic and aero-elastic models have been assessed comparing the critical instability temperatures and the panel flutter speed with results from literature. Finally the aero-thermo-elastic analysis of a FGM plate is performed.

### 3.1. Thermo-Elastic model assessment

A simply supported panel is considered to assess the thermo-elastic model. The geometry of the panel is reported in 2.

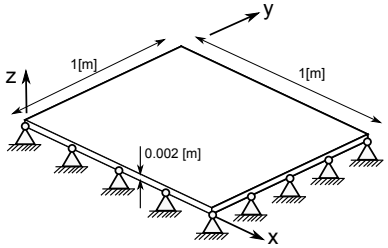


*Figure 2. Geometry of the simply supported pane*

The FGM mixtures law considered in this assessment is:

$$E(z) = (E_c - E_m)V_c(z) + E_m$$
$$\alpha(z) = (\alpha_c - \alpha_m)V(z) + \alpha_m$$
$$\nu(z) = \nu_0$$

where the subscript $c$ stand for the ceramic material and $m$ for the metallic.

| | $n_g$ | | | | |
|---|---|---|---|---|---|
| | 0 | 0.5 | 1 | 2 | 5 |
| ESL2 | 105.55 | 59.21 | 48.55 | 43.05 | 44.40 |
| ESL3 | 68.22 | 38.72 | 31.75 | 28.14 | 29.02 |
| ESL4 | 68.22 | 38.71 | 31.74 | 28.14 | 29.02 |
| LW2 | 105.55 | 59.21 | 48.55 | 43.05 | 44.40 |
| LW3 | 68.33 | 38.72 | 31.75 | 28.14 | 29.02 |
| LW4 | 68.22 | 38.71 | 31.74 | 28.14 | 29.02 |
| Ref. [6] | 68.02 | 38.65 | 31.70 | 28.09 | 28.96 |
| Ref. [12] | 70.7 | 39.48 | 32.27 | 28.53 | 29.33 |

*Table 1. $\Delta T_{cr}$ for different volume fraction index, $n_g$, evaluated using different structural models.*

Table 1 show the critical temperature of the panel for different values of volume fraction index evaluated using different structural models. The results are compared with those from literature. The present model provide a good accuracy in the evaluation of the critical temperature variation. When linear models are used, ESL2 and LW2, the results are non accurate therefore, at the least a quadratic model is required to achieve the expected results. When a single layer is considered LW models do not introduce any advantages with respect the ESL. When the volume fraction index increases, the percentage of aluminium in the FGM composition increases therefore a lower value of critical temperature is obtained.

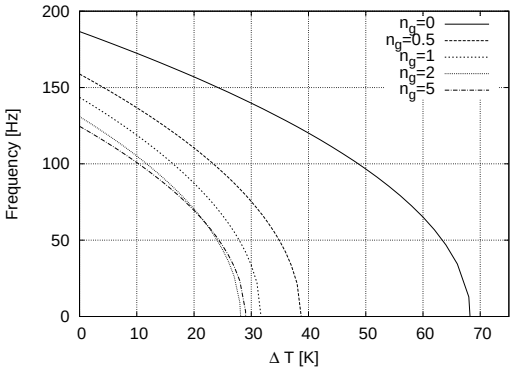


*Figure 3. First natural frequency Vs temperature.*

Figure 3 shows the evolution of the first natural frequency when the temperature is increased for different value of volume fraction index. This analysis shows that increasing the $n_g$ the natural frequency decrease. also when the temperature increases the natural frequency decreases, when the temperature reach the critical value the frequency becomes zero.

### 3.2. Aero-Elastic model assessment

The panel flutter speed of a simple isotropic panel, see Figure 4 has been investigated in order to assess the aeroelastic model. The panel is built using

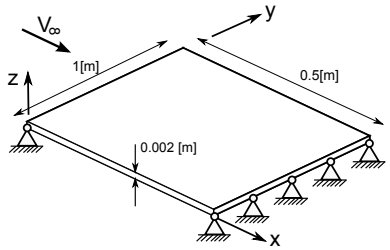


*Figure 4. Geometry and reference system of the panel use in the aeroelastic assessment.*

an aluminium alloy. The results in terms of critical Mach number and frequency are reported in Table 2. Different structural models have been considered.

| Model | $Ma_{cr}$ | $f_{cr}$ |
|---|---|---|
| Krause [13] | 4.5 | 66.03 |
| ESL2 | 4.39 | 65.46 |
| ESL3 | 4.36 | 65.31 |
| ESL4 | 4.36 | 65.31 |
| LW2 | 4.36 | 65.31 |
| LW3 | 4.36 | 65.32 |
| LW4 | 4.36 | 65.32 |

*Table 2. Panel flutter critical Mach and frequency fro different structural models.*

The results shows that both ,the ESL and the LW models, provide a good agreement with the reference results. A linear formulation is enough to ensure a good accuracy. Figure 5 show the evolution of

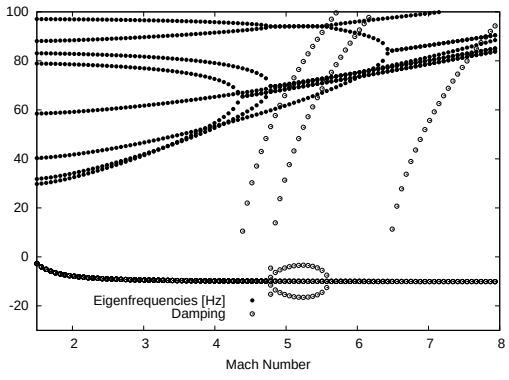


*Figure 5. Evolution of the natural frequencies and damping of the panel at different Mach numbers.*

the natural frequency and damping at different Mach numbers. The results show the classical aeroelastic instability, two frequency merge together and at the same speed the damping become positive making the panel unstable.

### 3.3. Aero-Thermo-Elastic Analysis of a FGM panel

In this section the aero-thermo-elastic model is considered. A square panel, see Figure 6, is considered. Two side are simply supported and two are free, therefore only the $\sigma_{xx^\theta}$ is considered. The FGM

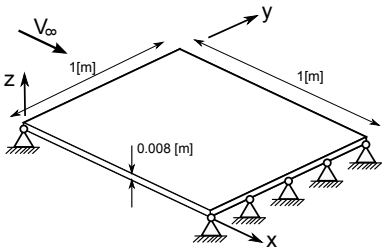


*Figure 6. Geometry and referecne system used in the aero-thermo-elastic analysis*

mixture equation are reported below, with $B$ is denoted the bulk modulus taht is strictly related with the elastic modulus. $\mu$ dentes the shear modulus.

$$\frac{B - B_m}{B_c - B_m} = \frac{V_c}{1 + (1 - V_c)\frac{B_c - B_m}{B_m + \frac{4}{3}\mu_m}} \tag{39}$$

$$\frac{\mu - \mu_m}{\mu_c - \mu_m} = \frac{V_c}{1 + (1 - V_c)\frac{\mu_c - \mu_m}{\mu_m + f_1}} \tag{40}$$

$$\frac{\alpha - \alpha_m}{\alpha_c - \alpha_m} = \frac{\frac{1}{B} - \frac{1}{B_m}}{\frac{1}{B_c}\frac{1}{B_m}} \tag{41}$$

Figure 7 show the instability boundaries of the panel when $n_g$ is equal to 5. In the lower part of the diagram are reported the evolution of the natural frequency before and after the critical temperature. If a non critical temperature is considered, the only instability which is present is the panel flutter instability, point A. When the temperature is greater than the critical value, in the first part of the dynamic pressure domain, from zero up to point $C$, the panel is buckled. Between the point $C$ and $B$ the panel is stable while, after the point $C$ a panel flutter phenomena arises. If all the temperature range is investigated a stability diagram can be drown, as the bigger one in Figure 7. The upper limits is given by the panel flutter phenomena, while the lower boundary arises from the buckling phenomena. Figure 8 show the stability boundary for different values of the volume fraction index. Higher is the alumina percentage, higher are the stability margin. This behaviour is due to the higher mechanical properties of the alumina with respect ti the aluminium.

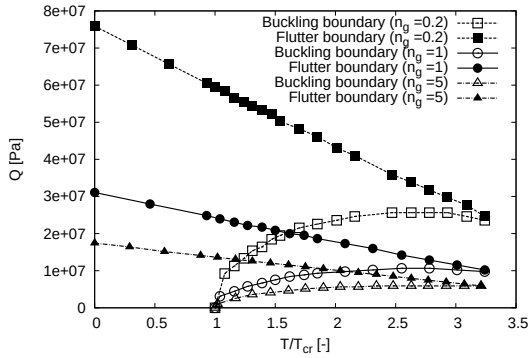


*Figure 8. Stability boundaries for different $n_g$ values.*

## 4. CONCLUSION

An advanced structural model able to deal with the aero-thermo-elastic problem has been developed in this work. The formulation has been developed in the framework of the Carrera Unified Formulaiton that allows the matrices to be written in compact form. Different structural models, Equivalent Single Layer and Layer-Wise, have been considered. The FGM material has been introduced in the formulation considering the mechanical and thermal properties not constant through the thickness. From the results it is possible to state that:

- The present model is able to include FGM material properly;
- The analysis of the aero-thermo-elastic problem require at the least a quadratic model;
- Aero-thermo-elastic analysis results show that a stability region can be detected where the panel is stable also at temperature higher that the critical temperature.
- The volume fraction index strongly afflict the performance of the panel.

the present model appears to be very promising in the analysis of FGM material and future works should be devoted to the refinement of the aerodynamic model and the introduction of non constant temperature over through the thickness.

## REFERENCES

[1] J.J Nichols. Final report: Saturn v, s-ivb panel flutter qualification test. *NASA-TN-D-5439*, 1969.

[2] E. Carrera, E. Zappino, G. Augello, A. Ferrarese, and M. Montabone. Aeroelastic analysis of versatile thermal insulation panels for

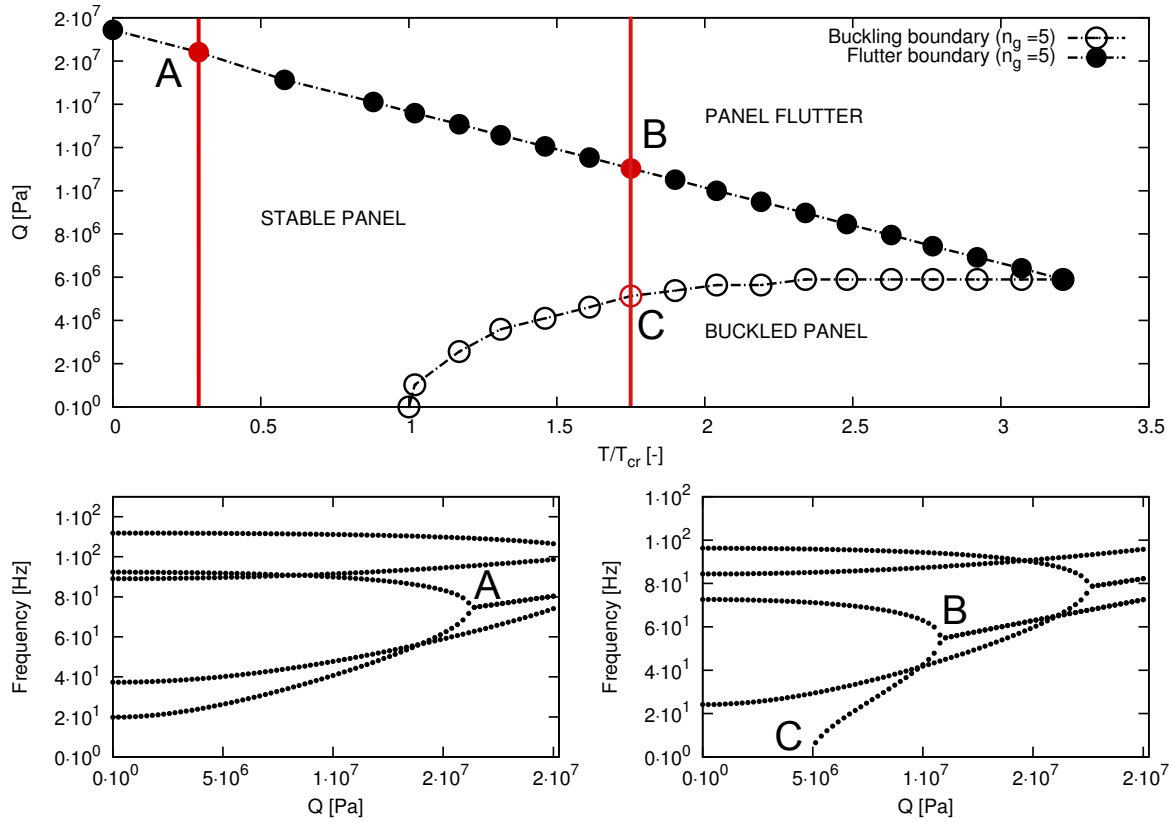


*Figure 7. Stability boundaries for different temperatures and dynamic pressure.*

launchers applications. In *7th European Symposium on Aerothermodynamics for Space Vehicles*, Brugges, Belgium, May 2011.

[3] E. Carrera, E. Zappino, K. Patocka, M. Komarek, A. Ferrarese, M. Montabone, B. Kotzias, B. Huermann, and R. Schwane. Aeroelastic analysis of versatile thermal insulation (vti) panels with pinched boundary conditions. *CEAS Space Journal*, 6(1):23–35, 2014.

[4] E. Carrera and E. Zappino. Aeroelastic analysis of pinched panel in variable supersonic flow changing with altitude. *Journal of Spacecraft and Rockets*, 51(1):187–199, 2014.

[5] F.A. Fazzolari and E. Carrera. Free vibration analysis of shandwich plates with asnisotropic face sheets in thermal environment by unsing hierarchical trigonometric ritz formulation. *Composites: Part B*, 50:67–81, 2013.

[6] A Fazzolari, F and E. Carrera. Thermal stability of fgm sandwich plates under various through-the-thickness temperature distributions. *Journal of Thermal Stresses*, 37:1449–1481, 2014.

[7] M. Cinefra, E. Carrera, L. Della Croce, and C. Chinosi. Refined shell elements for the analysis of functiionally graded structures. *Composite Structures*, 94(2):415–422, 2012.

[8] M. Cinefra, C. Chinosi, and L. Della Croce. Mitc9 shell elements based on refined theories for the analysis of isotropic cylindrical structures. *Mechanics of Advanced Materials ans Structures*, 20:91–100, 2013.

[9] H. Ashley and G. Zartarian. Piston theory - a new aerodynamic tool ffor the aeroelastician. *Composites Structures*, pages 1109–1118, 1956.

[10] E. Carrera, M. Cinefra, M. Petrolo, and E. Zappino. *Finite Element Analysis of Structures Through Unified Formulation*. John Wiley & Sons, 2014. In press.

[11] H. Krumhaar. The accuracy of linear piston theory when applied to cylindrical shells. *AIAA Journal*, 1:1448–1449, 1963.

[12] H. Nguyen-Xuan, Loc V. Tran, T. Nguyen-Thoi, and H.C. Vu-Do. Analysis of functionally graded plates using an edge-based smoothed finite element method. *Composite Structures*, 93(11):3019 – 3039, 2011.

[13] H. Krause. Flattern flacher schalen bei uberschallanstr omung. 1998.